

---

# EMERGENT MANIFOLD SEPARABILITY DURING REASONING IN LARGE LANGUAGE MODELS

---

Alexandre Polo<sup>\*1</sup>, Chanwoo Chun<sup>\*1,2</sup>, and SueYeon Chung<sup>1,3,4</sup>

<sup>1</sup>Department of Physics, Harvard University

<sup>2</sup>Center for Data Science, New York University

<sup>3</sup>Kempner Institute, Harvard University

<sup>4</sup>Center for Computational Neuroscience, Flatiron Institute  
{apolo, cchun}@g.harvard.edu, chung@fas.harvard.edu

February 25, 2026

## ABSTRACT

Chain-of-Thought (CoT) prompting significantly improves reasoning in Large Language Models, yet the temporal dynamics of the underlying representation geometry remain poorly understood. We investigate these dynamics by applying Manifold Capacity Theory (MCT) to a compositional Boolean logic task, allowing us to quantify the linear separability of latent representations without the confounding factors of probe training. Our analysis reveals that reasoning manifests as a transient geometric pulse, where concept manifolds are untangled into linearly separable subspaces immediately prior to computation and rapidly compressed thereafter. This behavior diverges from standard linear probe accuracy, which remains high long after computation, suggesting a fundamental distinction between information that is merely retrievable and information that is geometrically prepared for processing. We interpret this phenomenon as *Dynamic Manifold Management*, a mechanism where the model dynamically modulates representational capacity to optimize the bandwidth of the residual stream throughout the reasoning chain.

## 1 Introduction

Chain-of-Thought (CoT) prompting is highly effective at enabling Language Models (LMs) to solve complex compositional problems [Wei et al., 2022]. The intuition is that CoT distributes the computational load: rather than relying solely on feed-forward depth, the model utilizes the recursive generation of tokens to process information over time. However, the precise mechanisms governing this temporal processing remain largely uncovered.

In studying the information flow in feed-forward computation, investigating how the representation geometry evolves over layers has been proven to provide critical insights [Cohen et al., 2020, Pope et al., 2021]. However, not much is currently known about the evolution of the representation geometry over tokens. We bridge this gap by borrowing geometrical measures from computational neuroscience and deep neural networks (DNN) to track how internal computation unfolds over time.

Existing research on CoT internal representations often focuses on whether the textual output faithfully reflects the model’s hidden computation [Turpin et al., 2023, Lanham et al., 2023]. Recent works have used linear probes to show that intermediate answers are often linearly decodable well before they are generated [Zhang et al., 2025, Afzal et al., 2025]. However, standard probing techniques have inherent limitations that may lead to overestimating a model’s actual knowledge Afzal et al. [2025], and even show high accuracy when training on random features [Zhang and Bowman, 2018, Wieting and Kiela, 2019].

---

\*Equal contribution

To address these limitations, we analyze the latent space using Manifold Capacity Theory (MCT) [Chung et al., 2018] alongside linear probing. Unlike probing, MCT quantifies linear separability as an intrinsic geometric property, eliminating the need to train a classifier. This framework has provided key insights into information processing in visual and speech systems and early language models [Chou et al., 2024, Stephenson et al., 2019, 2021, Mamou et al., 2020, Kirsanov et al., 2025]

In this work, we use MCT to map the dynamics of representation manifolds in the residual stream during a compositional reasoning task (Figure 1).

Our core contributions are:

1. Geometric evidence, provided by Capacity Theory, that CoT involves active reasoning throughout generation, rather than only mimicking a reasoning trace.
2. LM dynamically modulates the representation geometry such that only the concepts that are relevant for a computation at a given time have high manifold capacity. We find that this mechanism keeps the representation dimensionality low, saving the bandwidth budget of the residual stream.

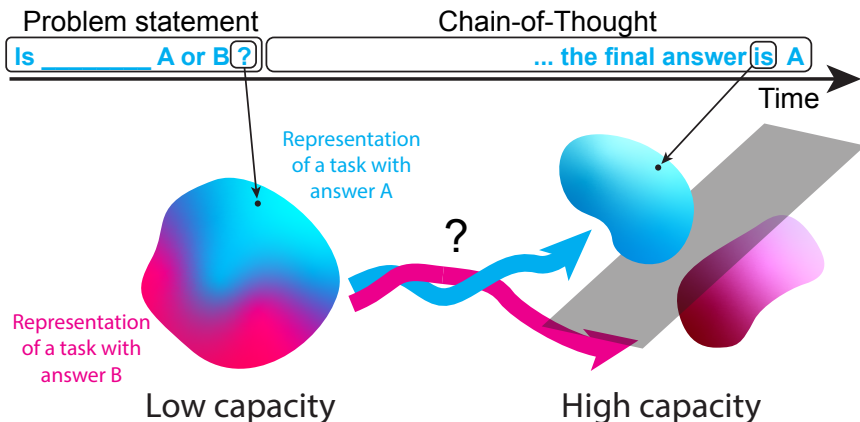


Figure 1: **Manifold Untangling during Chain-of-Thought.** Before any token is generated (left) the latent representations of tasks corresponding to answers A and B are entangled and hard to distinguish resulting in low capacity. As the model generates the CoT, it progressively untangles these representations. By the final token (right), the two manifolds are linearly separable and capacity is high.

## 2 Related Work

### 2.1 Internal Mechanisms of Chain-of-Thought

While the performance benefits of CoT are well-established, the nature of the underlying internal computation remains debated. One line of inquiry questions the *faithfulness* of the generated reasoning, suggesting that CoT may be a post-hoc rationalization rather than the actual causal driver of the prediction [Turpin et al., 2023, Lanham et al., 2023]. Smaller, distilled models may be particularly at risk of that, and it has been shown that for small models, more CoT granularity does not necessarily improve performance [Chen et al., 2025]. Conversely, recent interpretability work has identified a circuit within a two-layer attention-only model that plays a role in inductive reasoning [Elhage et al., 2021, Olsson et al., 2022].

A growing body of recent literature focuses specifically on decoding the reasoning states directly from the latent activations. Zhang et al. [2025] and Afzal et al. [2025] investigate the necessity of a long CoT and demonstrate that the correctness of an intermediate step is often linearly decodable long before the token is generated, suggesting that the model maintains a coherent internal truth state, and resulting in proposed early-stopping strategies.

Our work contributes to this discourse by looking for global geometric signatures of the reasoning steps, and specifically investigates the dynamics of the geometric representation along the CoT.

### 2.2 Linear Representations and Probing Challenges

The prevailing view in mechanistic interpretability is the *Linear Representation Hypothesis*, which suggests that neural networks encode semantic concepts such as sentiment, syntax, or factual truth—as vectors in a

linear subspace [Elhage et al., 2022]. Under this hypothesis, linear probes, supervised classifiers trained on frozen activations, have become a popular tool. They have been used to decode various concepts, from syntactic tree depth [Hewitt and Manning, 2019] to the truthfulness of model statements [Azaria and Mitchell, 2023, Burns et al., 2024, Marks and Tegmark, 2024], and even spatiotemporal coordinates [Gurnee and Tegmark, 2024], serving as a powerful diagnostic tool for locating information within the residual stream.

However, despite their empirical success, relying solely on probing accuracy presents significant methodological challenges. First, the probe is sensitive to regularization, optimizer, early stopping, class imbalance handling, and train/test splits. Moreover, Zhang and Bowman [2018], Wieting and Kiela [2019], and Hewitt and Liang [2019] established that linear probes can achieve high accuracy on random control tasks by exploiting the high-dimensional nature of the representation space or the structural priors of the model architecture. This has prompted the need to find a more geometric approach to interpretability research Afzal et al. [2025].

### 2.3 Manifold Theory and Representational Geometry

Geometry-based analysis techniques have been actively developed and widely used for studying the brain and the feed-forward networks [Pope et al., 2021, Lehky et al., 2014, Willett et al., 2021]. This approach treats a set of neural representations of inputs as a single entity: a neural manifold. The perspective that the goal of neural computation is to disentangle these manifolds (e.g., think of manifolds of dog images and cat images being disentangled in a vision network for the linear readout) has provided critical insights into the internal mechanism of the brain [DiCarlo and Cox, 2007].

This geometric perspective has been formalized through Manifold Capacity Theory [Chung et al., 2018, Cohen et al., 2020, Chou et al., 2024]. Manifold capacity quantifies the linear separability of these structures by applying principles from statistical mechanics. It is defined as the critical ratio  $\alpha = P/N^*$ , where  $P$  is the number of manifolds and  $N^*$  is the minimum dimensionality (of a random subspace to which the manifold is projected) required to achieve linear separation with a 50% probability. The theory also shows that  $\alpha$  is dependent on task-dependent geometric quantities, such as dimensionality and radius, providing a direct insight into what geometric properties of manifolds determine an observed  $\alpha$ . Essentially, it measures the efficiency of task-relevant feature encoding from the perspective of a linear downstream decoder. Crucially, by treating separability as an inherent geometric property, this framework eliminates the methodological pitfalls of probing.

This framework has previously been shown to provide useful insights into feedforward computation in the visual and auditory cortex [Chou et al., 2024], as well as in artificial vision models, where class manifolds are observed to progressively *untangle* over layers [Stephenson et al., 2019]. Figure 1 shows a schematic depiction of such untangling. However, its application to Large Language Models remains nascent. While Mamou et al. [2020] analyzed the geometry of static word embeddings and recent work has begun to explore the intrinsic dimension of transformer representations [Kirsanov et al., 2025], we extend this lineage by applying Manifold Capacity to the temporal dimension, tracking the dynamic modulation of concept manifolds during reasoning.

## 3 Methods

### 3.1 Compositional Boolean Logic Task

As a representative benchmark for tasks requiring multi-step reasoning, we utilize a hierarchical Boolean logic task. The goal is to evaluate the Boolean value of a nested expression, such as ((True and False) or (True xor True)). Each expression corresponds to a full binary tree of height  $h$ , where internal nodes represent logical operators AND, OR, XOR and leaf nodes provide Boolean constants.

To facilitate a structured analysis of the internal representations, we employ a consistent naming and ordering scheme. Each internal node is assigned a unique identifier [ID] based on a post-order or level-order traversal of the logic tree. This ensures that, with an appropriate prompt strategy, all tasks are solved in the same order. For our primary analysis on the internal representation, we generate a balanced dataset of 256 expressions (128 True, 128 False at the root) for a tree of height  $h = 5$ , containing  $2^h - 1 = 31$  internal nodes.

### 3.2 Prompting Strategy and Alignment

To capture the evolution of neural manifolds, we require the model to adhere to a rigid, structured output format using Markdown structural tokens. We prompt the model to reason through three distinct phases: *Problem Statement* (restating the expression and node IDs), *Solve* (step-by-step evaluation), and *Summary* (recalling all intermediate results).

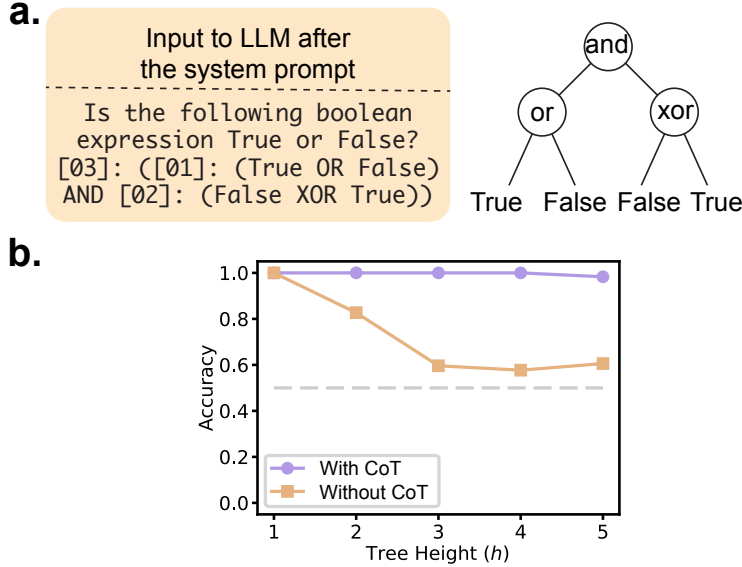


Figure 2: **a.** Example of a Boolean logic tree with height  $h = 2$ . *Left:* The corresponding text input provided to the model, where internal nodes are labeled [01] through [03]. *Right:* Schematic of the tree structure. **b.** Accuracy on Boolean logic trees of varying height. Performance with CoT (purple) remains near-perfect ( $> 98\%$ ), while standard prompting (No CoT, orange) degrades significantly as tree depth increases (61% for  $h = 5$ ). The dashed line marks the random baseline (50%).

The system prompt is designed to minimize formatting variance, allowing us to use the structural strings as *temporal anchors* for aligning representations across different tasks. We use the following condensed system prompt:

---

#### System Prompt for Structured Reasoning

---

You are a precise Boolean logic solver. You will be given a boolean expression where specific operations are labeled with IDs like [01], [02], etc.

Your task is to solve the tree step-by-step in strictly **increasing order** of these IDs. Follow the exact format shown in the example below.

### EXAMPLE OUTPUT:

### Problem Statement

1. **Expression**: '[03]: ([01]: (True or False) and [02]: (False xor True))'

2. **Node IDs**: [01], [02], [03]

### Solve

**Node [01]**

\* Logic: 'True or False'

\* Result: 'True'

**Node [02]**

\* Logic: 'False xor True'

\* Result: 'True'

**Node [03]**

\* Logic: '[01] and [02]'  $\rightarrow$  'True and True'

\* Result: 'True'

### Summary

\* [01]: True

\* [02]: True

\* [03]: True

**Final Answer: True**

### YOUR TURN:

---

This structured output serves a dual purpose: it improves model accuracy (achieving 98% accuracy on depth-5 tasks with *Ministral 3 8B Reasoning*) and provides deterministic textual markers to compute the manifold capacity  $\alpha_t^{(n)}$  at semantically equivalent points in the reasoning chain. While such a precise description of the task to the model arguably simplifies the reasoning the model has to do, it allows us to focus more clearly on the memory management aspect of the task.

### 3.3 Model Configuration

For all experiments, we utilize the *Minstral 3 8B Reasoning* model Liu et al. [2026], a state-of-the-art small language model specifically optimized for complex, multi-step reasoning tasks. The model consists of 32 transformer layers and its residual stream is of dimension 4096. Note that the model family has been distilled from Mistral Small 3.1. To ensure deterministic reasoning and stable manifold geometry across all tasks, we set the temperature to  $T = 0.0$  and disable sampling. All experiments are executed on NVIDIA A100 (80GB) GPUs, utilizing the eager attention implementation for consistent activation capturing across the residual stream.

### 3.4 Structural Token Anchoring and the Contamination Problem

A primary challenge in analyzing neural manifolds during CoT is the issue of *textual contamination*. Because the model’s response explicitly contains the answers to intermediate sub-problems, any measurement of the encoded state taken at the exact token where a solution is articulated (e.g., the token for "True" in "Node [01] Result: True") would be trivial. Such a signal would merely reflect the model’s *reading* of its own generated text rather than its internal reasoning process.

To circumvent this, we restrict our manifold capacity calculations and linear probing to specific **structural anchors**. These anchors are formatting strings (e.g., ### Solve, \* Logic:) that precede the actual solution of a node. We focus our analysis on the **final token** of each structural string for three primary reasons:

1. **Causal Independence (Leakage Prevention):** By measuring capacity at the token right *before* the textual solution is generated, we ensure that the linear separability we observe is an emergent property of the latent representation rather than a reflection of the output token itself.
2. **Contextual Aggregation:** The last token of a structural string (e.g., the colon in \* Result:) serves as the point of maximum contextual pressure where the model must aggregate information to produce the next logical result.
3. **Semantic Alignment:** Using fixed formatting strings provides a common time, allowing us to align trajectories across tasks that generate a varying number of tokens.

This methodology allows us to focus our attention on the internal computation.

### 3.5 Analysis Methods

To solve the task it is asked, the model has to successively determine the truth value of each node. At any point in the CoT generation, at any layer in the model, one can group the activations with respect to the truth value of any node in order to decode the extent to which the information about that node’s value is being encoded. This decoding can be done through the lens of manifold capacity theory or with a linear probe. The tokens along the CoT generation that we analyze are the structural tokens described in the above subsection.

**Manifold Capacity** We measure the manifold capacity on a set  $\mathcal{M} := \{\mathbf{x}_i\}_{i=1}^D$  of intermediate layer residual stream embeddings aligned at a single structural token across  $D$  number of Boolean logic problems, with classification labels  $\mathcal{Y} := \{y_i\}_{i=1}^D$  specified as the ground truth answers to a single node in the Boolean logic tree.

The MCT tells us that  $N^*$ , the minimal random subspace dimensions needed for linear separation according to some labeling, can be efficiently computed by [Chou et al., 2024]

$$N^* = \left\langle \|\Pi_{\mathcal{V}}(\mathbf{t})\|_2^2 \right\rangle_{\mathbf{t} \sim \mathcal{N}(0, \mathbf{I}_N)},$$

where  $\Pi_{\mathcal{V}}(\mathbf{t})$  is a Euclidean projection of the  $\mathbf{t}$  vector to a cone  $\mathcal{V}$  of the points  $\{y_i \mathbf{x}_i\}_{i=1}^D$  where  $y_i$  is 1 if the ground truth answer of a given node is True, and  $-1$  if False. In our work, we simply set  $P = 2$  when computing  $\alpha$ , i.e.  $\alpha = 2/N^*$ .

**Linear Probes** To complement the capacity measure, we employ linear probes trained to separate the same manifolds. We utilize two distinct linear classifiers: a Hard-Margin Support Vector Machine (SVM) and Logistic Regression. Given that the high-dimensional representations in our analysis are linearly separable, the Hard-Margin SVM serves as a direct geometric probe.

Note that the training of the hard-margin SVM yields a maximum margin hyperplane. The direction of a normal vector to this hyperplane can be used as a representative direction of the encoding of the truth value of the node in question at

that particular time. This then allows us to look at whether this direction for a given node is conserved over time, and to look at cosine similarity measures of the direction across nodes (for an accordingly chosen time, which should be node-dependent).

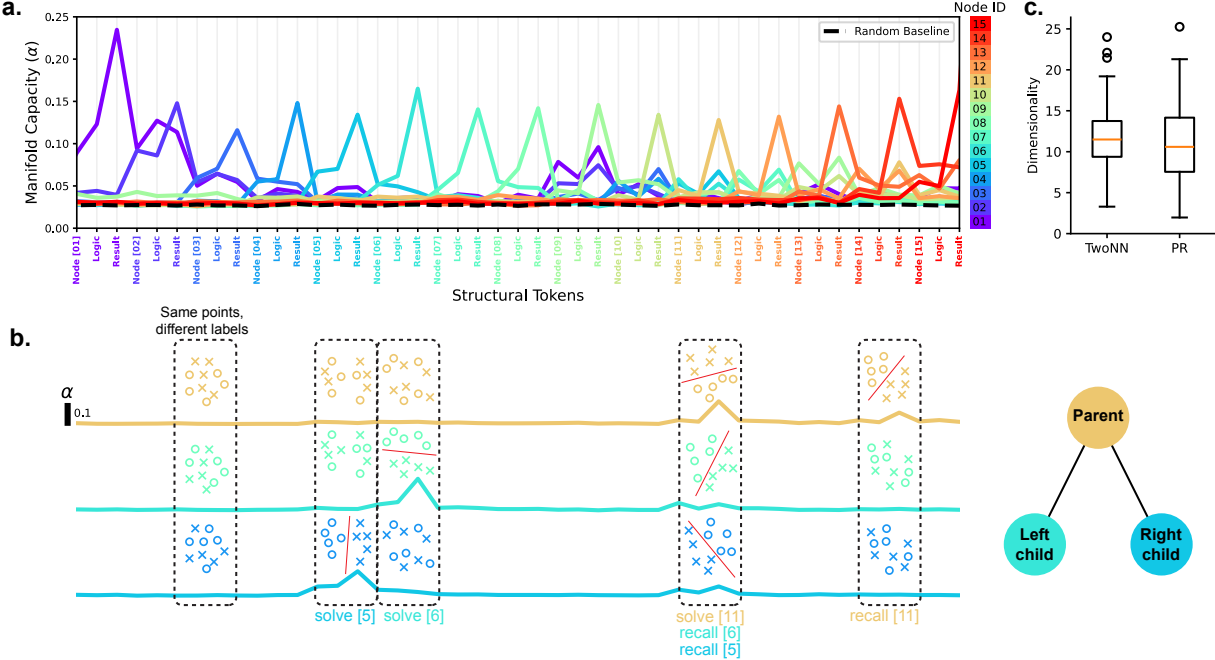


Figure 3: **Dynamic Modulation of Manifold Geometry during CoT.** **a.** Manifold capacity ( $\alpha$ ) tracked across the Chain-of-Thought sequence (layer 20, tree height  $h = 4$ , see Supplementary for height 5). Lines are colored by node ID. Capacity for a specific node peaks sharply at two distinct moments: first when the node is intrinsically computed, and second when it is processed by its parent. **b.** Detailed analysis of Node 11 (yellow) and its children, Node 5 (blue) and Node 6 (turquoise). Insets visualize the latent geometry at key timesteps. High capacity peaks correspond to linearly separable manifolds (clear decision boundaries). Notably, representations become entangled (low capacity) in the interim periods between the initial solution (solve) and the subsequent retrieval (recall). **c.** Intrinsic dimensionality estimates of the latent embeddings using Two-Nearest Neighbors (TwoNN) and Participation Ratio (PR).

## 4 Results

We analyze the geometry of the residual stream during reasoning on our tree boolean logic task. We first validate the model’s performance, then track the evolution of Manifold Capacity and Probe Accuracy over time (tokens) and space (layers).

### 4.1 Task Performance

On the depth-5 Boolean Logic task, *Ministral 3 8B Reasoning* achieves 98% accuracy with full CoT generation, compared to 59% (barely above random guess) when prompted for an immediate answer (cf. Fig.2b). This confirms that CoT is functionally necessary for this architecture to solve the task, and ensures that our subsequent analysis reflects correct reasoning traces.

### 4.2 Dynamic Manifold Management

We track the representation geometry through the generation of the CoT through the lens of manifold capacity and linear probes. Through this we aim to exhibit a signature of the reasoning process taking place and unveil specific aspects of its dynamics.

We first look at the evolution of our metrics at layer 20 of the model, as it is in the mid to late layers that it is thought most of the reasoning actually takes place. The next subsection attends to a more specific layer  $\times$  time analysis.

**Computation Signal** We observe that linear separability is not a static property of the representation but follows a distinct pulse-like trajectory. As shown in Figure 3ab, we see that the capacity measured by a given node’s ground truth answer, namely a “node capacity”, spikes when that node is being solved, and then decays back to the baseline. This is in contrast to an alternative possibility that each node’s capacity stays up after the node is solved. Essentially, the information about the solution of a node is erased from the residual stream immediately after being solved, to create bandwidth for the subsequent node to be solved. Later, when the node is recalled to solve its parent node, the capacity spikes again, but to a lesser degree Figure 3ab.

Since the LM manages the representations such that only a small number of relevant concepts are separable (the two children node answers, and the current node’s answer) at a given time, the dimensionality of the representation can be kept small, assuming that each concept takes different directions according to the Linear Representation Hypothesis. This is reflected by our estimations of both the local (intrinsic) and global dimensionalities, measured by the TwoNN and participation ratios, respectively (Figure 3c). Across the entire CoT, both dimensionalities hover around just 10.

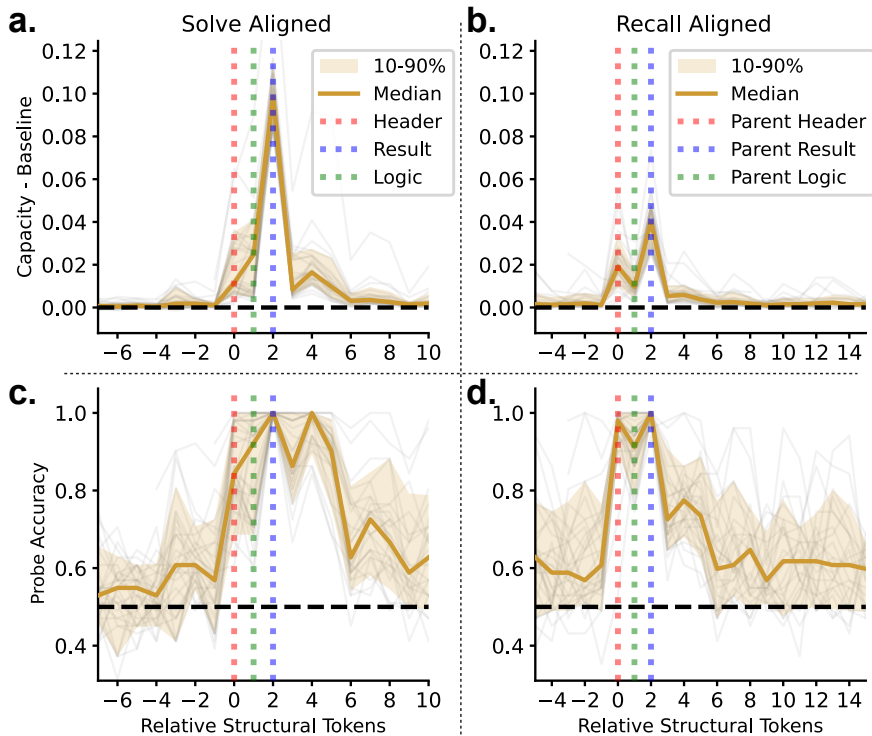


Figure 4: **Dynamics of separability metrics during Solve and Recall events.** Data is aligned to the moment a node is computed (Left column: **a**, **c**) or when it is recalled by its parent (Right column: **b**, **d**). (**a**, **b**) *Manifold Capacity*: Shows a sharp, transient peak at the moment of computation and recall, dropping quickly to baseline in between. (**c**, **d**) *Hard-margin SVM probe test accuracy*: While accuracy also peaks at computation, it exhibits a sustained plateau, decaying much slower than capacity. Vertical dashed lines mark the relative positions of structural tokens (Header, Result, Logic).

To reveal a fine-grained pattern of the canonical trace of the node capacity at the node’s solve phase and recall phase, we align the traces at the solve phase structural tokens Figure 4a, and at the recall phase structural tokens Figure 4b. There are three structural tokens, i.e. “header”, “logic”, and “result”, in each phase. We see that the capacity for a target node peaks at the structural tokens immediately *preceding* the generation of the textual answer. The increase in separability begins as soon as the model generates the tokens corresponding to the node’s dependencies. This indicates that the linear separability of the concept emerges in the residual stream prior to the explicit token decoding.

**Separability Decay and Divergence with Linear Probes** Immediately after a node’s computation is complete, its Manifold Capacity decays rapidly (Figure 4b). This marks a divergence compared to the accuracy of a Linear Probe and an SVM trained on the same features. While the probe accuracy remains high ( $> 90\%$ ) for the tokens corresponding to the next two nodes being computed, the Manifold Capacity drops near the random baseline. This divergence highlights a difference between the information recoverable by a trained classifier and the information available via linear separation in the current geometry. However, as shown in the Supplementary section, the signal is much noisier and weaker with

the probes, and it can only be revealed when the traces are aligned Figure 4cd (the result for SVM is shown here; the result for Logistic Regression can be found in the Supplementary section).

### 4.3 Spatiotemporal Localization

We extended our analysis to the full Layer  $\times$  Time grid to locate the physical origin of these geometric pulses. Given that the model recreates its residual stream at every token, this allows us to see how the model chooses to expand or not any given piece of information that it might want to do computations on across the layers.

Figure 5 presents the capacity change averaged over all nodes along the reasoning trace, aligned with respect to the moment where the node is solved. We identify two distinct phases:

1. **Reasoning Phase:** At the *header* and *logic* structural tokens of a specific node, the increase in separability originates in the middle layers (Layers 13-15). Then at the *result* structural token (immediately before the answer is spelled out), the capacity strongly increases throughout all layers.
2. **Reorganization Phase:** In the subsequent tokens that pertain to the next node’s computation, the evolution is dramatically different. While early layers maintain higher capacity (likely retaining the immediate context), the middle layers (13-15) show a rapid decrease in capacity for the previous node, so that in the later layers (16-32) the information is not readily accessible anymore.

A similar behavior can be seen when looking at the linear probes test accuracy (Figure S.2) for the reasoning phase, however the suppression phase is a lot less marked for them, and the probe accuracy hovers above 90% in later layers for up to two nodes after the computation is done.

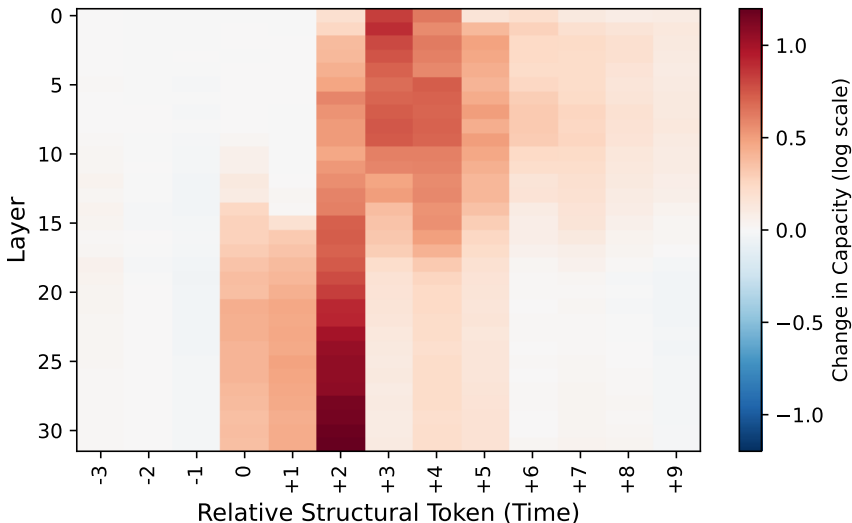


Figure 5: **Spatiotemporal heatmap of manifold capacity change.** The x-axis represents token positions relative to the computation step ( $t = 0$ ). (*During Computation*,  $t = 0, 1$ ) A capacity increase initiates in the middle layers at  $t = 0$ , culminating in a sharp peak within the deep layers at the token preceding the result ( $t = +2$ ). (*Post-Computation*) For  $t > +2$ , the early-to-mid layers retain elevated capacity as they retain the immediate context; however, this capacity decreases in the middle layers as the model reorganizes its representation to shift focus to the next node.

### 4.4 Implicit Compositionality (Silent CoT)

Does the capacity of a node increase when the node is being recalled, simply because it needs to write down that node’s truth value (or even the name) during the recall phase, or because of computational need? To check this, we prompted Ministral to silence the textual output of the child node names or values during CoT (see S.I. B). We observe that the child nodes’ capacities still spike during the recall phases, strongly indicating that these spikes are for the internal computations, not simply for the textual output.

### 4.5 Directions of Separation

We saw in Figure 3c that the dimensionality is kept low during CoT, and only a few concepts are separable, minimizing the bandwidth of the residual stream. The question is, what exactly takes up how much space in the residual stream

bandwidth during computation? To test this in our setup, we investigate the directions orthogonal to the max-margin separating hyperplanes.

Figure 3 shows that when a node is being solved, the manifold is separable by the answers of both the left and right child nodes. Interestingly, we find that there are two strongly conserved directions for separating the left and right child node answers, and they are slightly pointing in opposite directions, taking at least two dimensions (Figure S.7-right). The fact that the left and right child node directions are strongly conserved indicates the LM truly solves the problem in a compositional manner, applying the same local rule across subproblems. Since the manifold needs to be separated with respect to the parent node as well, the minimum number of dimensions required for the computation is three. In addition, we find that the direction that separates a node’s answer while it is being solved is not conserved across nodes (Figure S.7-left). Moreover, the directions in which the node is solved and recalled are also not conserved (Figure S.8). See Section C for more details.

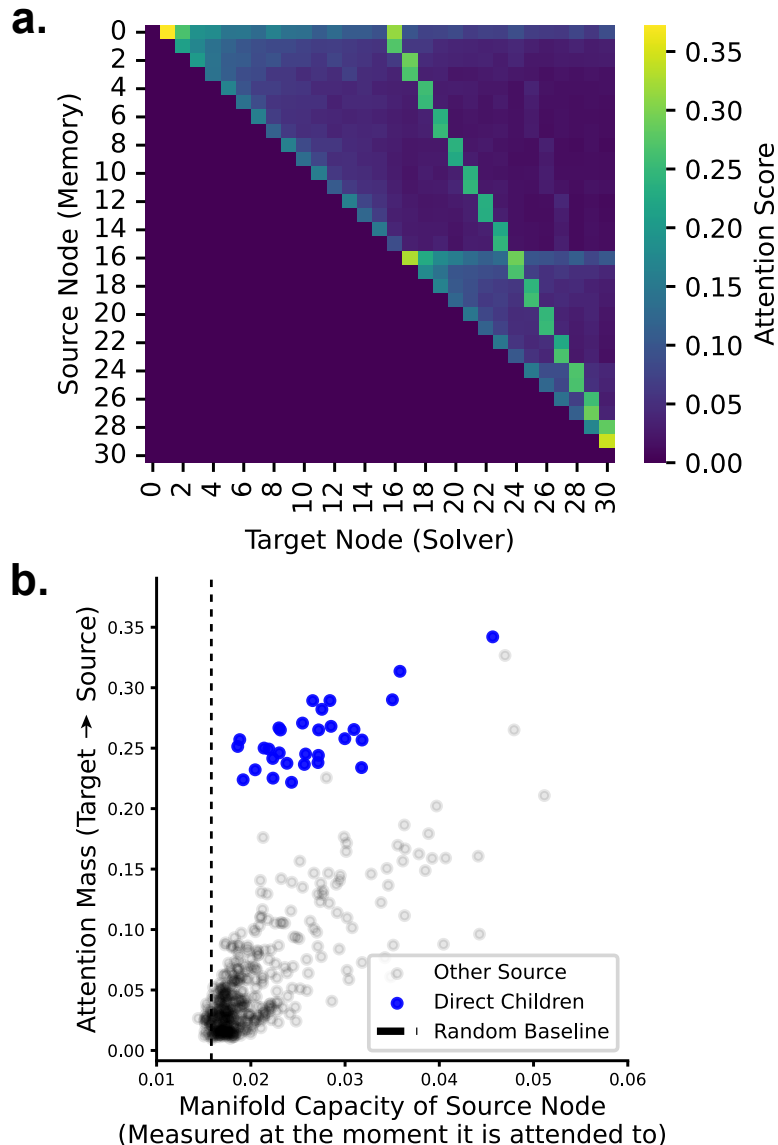


Figure 6: **Correlation between Attention and Manifold Capacity.** **a.** Attention score heatmap between graph nodes. The x-axis represents the target node currently being solved; the y-axis represents the source nodes in the context. The diagonal structure reflects the model attending to recent context, while off-diagonal points represent the retrieval of specific dependencies. **b.** Scatter plot of Attention Score versus Manifold Capacity of the source node at the moment of attention. We observe a strong positive correlation ( $r = 0.723$ ), specifically for direct children nodes (blue), indicating that the model preferentially attends to previous information when its representation is linearly separable.

#### 4.6 Attention Modulates Capacity

We see in Figure 4a that the node capacity drops to the baseline after the node is solved and spikes again when it is recalled. Does this mean the information about the intermediate answer is erased in the residual stream after solving? Or does the information somehow still exist in the residual stream but cannot be linearly decoded?

We answer this by investigating attention. If the information is lost in the residual stream, the attention mechanism will fetch it back from the embeddings of the earlier tokens. Our analysis of the attention strongly suggests this. When the current node is being solved, the attention strengths the current token (i.e., target token) has on the solve phase (i.e., source token) of the children nodes are conspicuously strong Figure 6a. The exact method of quantifying the attention score is explained in the Supplementary section.

Strikingly, we find that the strength of attention to a previously visited concept (source) is highly correlated with the capacity of that concept at the target Figure 6b. In summary, these observations suggest that the strategic management of the representation geometry is mediated by the attention mechanism of the LM.

### 5 Discussion

Our analysis reveals the existence of precise, complex dynamical processes throughout the CoT, which we interpret as signatures of the reasoning taking place. Relevant information is encoded as linearly separable manifolds, and is modulated in a highly efficient, time-sensitive manner. Rather than maintaining a static representation of all logical variables, the model successively renders accessible only the information required for the immediate computational step.

Our investigation into the internal dynamics of CoT offers a geometric insight into the debate regarding the *faithfulness* of intermediate reasoning steps. By analyzing the dynamic evolution of Manifold Capacity, we uncover a distinct signature of computation: reasoning manifests as the transient *untangling* of semantic manifolds.

**Geometric Signatures of Active Computation** Addressing the open question of whether CoT is a post-hoc rationalization or a causal driver [Turpin et al., 2023], our results support the latter. We observe a *pre-computation signal* where the manifold capacity for a specific logical node peaks immediately prior to the generation of the answer tokens. This precise temporal synchronization suggests that the model is not simply mimicking a reasoning trace, but is actively modulating the geometry of its residual stream to render specific information linearly accessible exactly when the computation requires it. This pulsing behavior acts as a geometric signature of the reasoning process, distinguishing functional computation from inert representation.

**Retention vs. Readiness of Information** A key finding of our study is the point where Manifold Capacity and standard Linear Probes diverge. While probes maintain high accuracy long after a computational step is finished, Manifold Capacity in the decays rapidly.

We propose that these two metrics capture different states of information. High probe accuracy indicates *retention*: the information remains encoded in the high-dimensional latent space. High manifold capacity indicates *readiness*: the information is explicitly structured for linear readout, enabling computations to happen. Combined with the direction analysis, this rapid decay of capacity suggests a mechanism of subspace rotation: once a logical step is over, the model rotates the representation out of the primary linear subspace used for computation.

This acts as cleaning the active workspace to prevent past variables from interfering with the current logical operation. While past data doesn’t need to be fully suppressed and can still be recovered by a linear probe, it appears to be effectively archived and not ready for computation.

**Spatiotemporal Dynamics and the Locus of Reasoning** Our layer-wise analysis reinforces this view of a dynamic workspace by specifying the flow of information across layers at the different time points. We observe that increases in manifold capacity originate in the middle-to-late layers (13–16) during the processing of a step, as soon as the models starts discussing a specific node. Crucially, the early layers only exhibit high capacity for that same node in the *subsequent* tokens after the answer is generated. The fact that the geometric signature emerges first in the deep layers of the current token, and is only reflected in the shallow layers of the next token, confirms a causal chain where computation precedes representation. This supports the view of a specialization of the layers of the network Elhage et al. [2021] where the early layers prepare the workspace (the residual stream) so that the later one can do the actual computation, with the residual stream making the link between all.

**Dynamic Manifold Management** We interpret these combined dynamics—the localized pulses, the subspace rotation, the layer specialization and the attention correlation—as a unified mechanism of *Dynamic Manifold Management*. For reasoning tasks with high compositionality, the fixed dimensionality of the residual stream becomes a central constraint. A static representation of a complex reasoning tree would require maintaining linearly separable directions for every intermediate variable simultaneously, quickly exhausting the available spatial bandwidth. Instead CoT allows the model to distribute computational load across time. It optimizes the geometry of its residual stream by expanding relevant concepts into separable manifolds *only* during the moment of computation, and compressing them immediately afterward to save space and attend to the next computation without interference. This supports the view of the residual stream as a global workspace: the model uses the generated text to offload information, retrieving and processing it in the middle layers only when necessary.

## Limitations

Our study uses a synthetic Boolean logic task, which offers precise structural control but lacks the ambiguity of natural language. It remains for future works to see if the rigid pulse dynamics we observed transfer to unstructured domains or larger models (e.g., 70B+ parameters) with wider residual streams. Additionally, our reliance on Manifold Capacity assumes the model primarily uses linear separability for internal steps. While the Linear Representation Hypothesis is common, LMs may also rely on non-linear geometries that our current metrics do not fully capture.

## Acknowledgements

We thank Abdulkadir Canatar for early discussions, Yonatan Belinkov and Kyunghyun Cho for insightful feedback, and Manu Srinath Halvagal and Artem Kirsanov for helpful comments. This work is supported by the Samsung Advanced Institute of Technology (under the project "Next Generation Deep Learning: From Pattern Recognition to AI"). S.C. is also supported by the Klingenstein-Simons Award, and a Sloan Research Fellowship.

## Impact Statement

Reliable mechanistic interpretability is a prerequisite for AI safety. By demonstrating that Chain-of-Thought induces geometrically separable feature manifolds, our work provides a foundation for detecting truthful reasoning in Large Language Models. Our application of Manifold Capacity Theory offers a more rigorous alternative to standard linear probing methods, mitigating the risk of overestimating a model’s active knowledge.

## References

- Anum Afzal, Florian Matthes, Gal Chechik, and Yftah Ziser. Knowing before saying: Llm representations encode information about chain-of-thought success before completion. *arXiv preprint arXiv:2505.24362*, 2025.
- Amos Azaria and Tom Mitchell. The internal state of an llm knows when it’s lying. *arXiv preprint arXiv:2304.13734*, 2023.
- Collin Burns, Haotian Ye, Dan Klein, and Jacob Steinhardt. Discovering latent knowledge in language models without supervision. *arXiv preprint arXiv:2212.03827*, 2024.
- Xinghao Chen, Zhijing Sun, Guo Wenjin, Miaoran Zhang, Yanjun Chen, Yirong Sun, Hui Su, Yijie Pan, Dietrich Klakow, Wenjie Li, and Xiaoyu Shen. Unveiling the key factors for distilling chain-of-thought reasoning. In *Findings of the Association for Computational Linguistics: ACL 2025*, pages 15094–15119. Association for Computational Linguistics, July 2025. doi: 10.18653/v1/2025.findings-acl.782.
- Chi-Ning Chou, Royoung Kim, Luke A Arend, Yao-Yuan Yang, Brett D Mensh, Won Mok Shim, Matthew G Perich, and SueYeon Chung. Geometry linked to untangling efficiency reveals structure and computation in neural populations. *bioRxiv*, pages 2024–02, 2024.
- SueYeon Chung, Daniel D Lee, and Haim Sompolsky. Classification and geometry of general perceptual manifolds. *Physical Review X*, 8(3):031003, 2018.
- Uri Cohen, SueYeon Chung, Daniel D Lee, and Haim Sompolsky. Separability and geometry of object manifolds in deep neural networks. *Nature communications*, 11(1):746, 2020.
- James J. DiCarlo and David D. Cox. Untangling invariant object recognition. *Trends in Cognitive Sciences*, 11(8): 333–341, 2007.

- Nelson Elhage, Neel Nanda, Catherine Olsson, Tom Henighan, Nicholas Joseph, Ben Mann, Amanda Askell, Yuntao Bai, Anna Chen, Tom Conerly, et al. A mathematical framework for transformer circuits. *Transformer Circuits Thread*, 1(1):12, 2021.
- Nelson Elhage, Tristan Hume, Catherine Olsson, Nicholas Schiefer, Tom Henighan, Shauna Kravec, Zac Hatfield-Dodds, Robert Lasenby, Dawn Drain, Carol Chen, Roger Grosse, Sam McCandlish, Jared Kaplan, Dario Amodei, Martin Wattenberg, and Christopher Olah. Toy models of superposition. *arXiv preprint arXiv:2209.10652*, 2022.
- Wes Gurnee and Max Tegmark. Language models represent space and time. *arXiv preprint arXiv:2310.02207*, 2024.
- John Hewitt and Percy Liang. Designing and interpreting probes with control tasks. *arXiv preprint arXiv:1909.03368*, 2019.
- John Hewitt and Christopher D. Manning. A structural probe for finding syntax in word representations. In *Proceedings of the 2019 Conference of the North American Chapter of the Association for Computational Linguistics: Human Language Technologies, Volume 1 (Long and Short Papers)*, pages 4129–4138. Association for Computational Linguistics, June 2019.
- Artem Kirsanov, Chi-Ning Chou, Kyunghyun Cho, and SueYeon Chung. The geometry of prompting: Unveiling distinct mechanisms of task adaptation in language models. *arXiv preprint arXiv:2502.08009*, 2025.
- Tamera Lanham, Anna Chen, Ansh Radhakrishnan, Benoit Steiner, Carson Denison, Danny Hernandez, Dustin Li, Esin Durmus, Evan Hubinger, Jackson Kernion, Kamilė Lukošūtė, Karina Nguyen, Newton Cheng, Nicholas Joseph, Nicholas Schiefer, Oliver Rausch, Robin Larson, Sam McCandlish, Sandipan Kundu, Saurav Kadavath, Shannon Yang, Thomas Henighan, Timothy Maxwell, Timothy Telleen-Lawton, Tristan Hume, Zac Hatfield-Dodds, Jared Kaplan, Jan Brauner, Samuel R. Bowman, and Ethan Perez. Measuring faithfulness in chain-of-thought reasoning. *arXiv preprint arXiv:2307.13702*, 2023.
- Sidney R Lehky, Roozbeh Kiani, Hossein Esteky, and Keiji Tanaka. Dimensionality of object representations in monkey inferotemporal cortex. *Neural computation*, 26(10):2135–2162, 2014.
- Alexander H. Liu, Kartik Khandelwal, Sandeep Subramanian, Victor Jouaul, et al. Ministral 3. *arXiv preprint arXiv:2601.08584*, 2026.
- Jonathan Mamou, Hang Le, Miguel A Del Rio, Cory Stephenson, Hanlin Tang, Yoon Kim, and SueYeon Chung. Emergence of separable manifolds in deep language representations. In *Proceedings of the 37th International Conference on Machine Learning*, pages 6713–6723, 2020.
- Samuel Marks and Max Tegmark. The geometry of truth: Emergent linear structure in large language model representations of true/false datasets. *arXiv preprint arXiv:2310.06824*, 2024.
- Catherine Olsson, Nelson Elhage, Neel Nanda, Nicholas Joseph, Nova DasSarma, Tom Henighan, Ben Mann, Amanda Askell, Yuntao Bai, Anna Chen, Tom Conerly, Dawn Drain, Deep Ganguli, Zac Hatfield-Dodds, Danny Hernandez, Scott Johnston, Andy Jones, Jackson Kernion, Liane Lovitt, Kamal Ndousse, Dario Amodei, Tom Brown, Jack Clark, Jared Kaplan, Sam McCandlish, and Chris Olah. In-context learning and induction heads. *arXiv preprint arXiv:2209.11895*, 2022.
- Phillip Pope, Chen Zhu, Ahmed Abdelkader, Micah Goldblum, and Tom Goldstein. The intrinsic dimension of images and its impact on learning. *arXiv preprint arXiv:2104.08894*, 2021.
- Cory Stephenson, Jenelle Feather, Suchismita Padhy, Oguz Elibol, Hanlin Tang, Josh McDermott, and SueYeon Chung. Untangling in invariant speech recognition. *Advances in neural information processing systems*, 32, 2019.
- Cory Stephenson, Suchismita Padhy, Abhinav Ganesh, Yue Hui, Hanlin Tang, and SueYeon Chung. On the geometry of generalization and memorization in deep neural networks. *arXiv preprint arXiv:2105.14602*, 2021.
- Miles Turpin, Julian Michael, Ethan Perez, and Samuel R. Bowman. Language models don’t always say what they think: Unfaithful explanations in chain-of-thought prompting. *arXiv preprint arXiv:2305.04388*, 2023.
- Jason Wei, Xuezhi Wang, Dale Schuurmans, Maarten Bosma, Fei Xia, Ed Chi, Quoc V Le, Denny Zhou, et al. Chain-of-thought prompting elicits reasoning in large language models. *Advances in neural information processing systems*, 35:24824–24837, 2022.
- John Wieting and Douwe Kiela. No training required: Exploring random encoders for sentence classification. *arXiv preprint arXiv:1901.10444*, 2019.
- Francis R Willett, Donald T Avansino, Leigh R Hochberg, Jaimie M Henderson, and Krishna V Shenoy. High-performance brain-to-text communication via handwriting. *Nature*, 593(7858):249–254, 2021.
- Anqi Zhang, Yulin Chen, Jane Pan, Chen Zhao, Aurojit Panda, Jinyang Li, and He He. Reasoning models know when they’re right: Probing hidden states for self-verification. *arXiv preprint arXiv:2504.05419*, 2025.

Kelly W Zhang and Samuel R Bowman. Language modeling teaches you more syntax than translation does: Lessons learned through auxiliary task analysis. *arXiv preprint arXiv:1809.10040*, 2018.

### A Additional Separability Measures

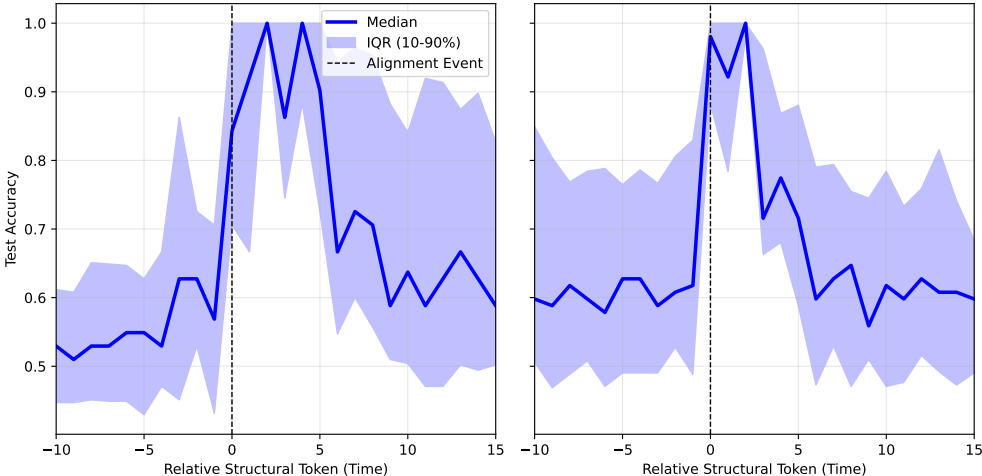


Figure S.1: **Spatiotemporal heatmap of Hard-Margin SVM Test Accuracy.** (Layer 20) The x-axis represents token positions relative to the computation step ( $t = 0$ ). (*During Computation*,  $t = 0, 1$ ) The test accuracy increase initiates in the middle layers at  $t = 0$ , culminating in a value close to 1 across layers at the token preceding the result ( $t = +2$ ). (*Post-Computation*) For  $t > +2$ , the early-to-mid layers retain close to 1 accuracy as they retain the immediate context; the accuracy decreases in the middle layers of the model but not very markedly. Only at the subsequent node ( $t > +5$ ) is the decrease more pronounced.

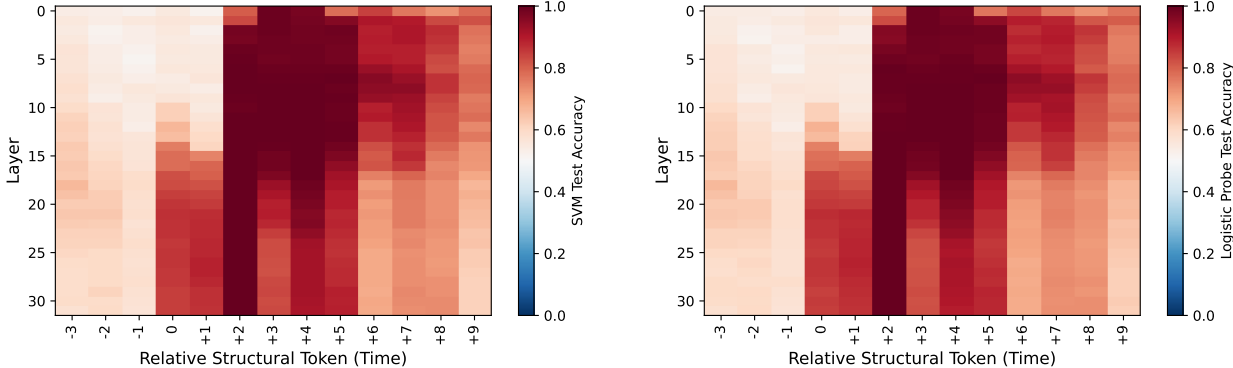


Figure S.2: **Spatiotemporal heatmap of Test Accuracy.** **Left:** Hard-Margin Support Vector Machine. **Right:** Logistic Probe. The x-axis represents token positions relative to the computation step ( $t = 0$ ). (*During Computation*,  $t = 0, 1$ ) The test accuracy increase initiates in the middle layers at  $t = 0$ , culminating in a value close to 1 across layers at the token preceding the result ( $t = +2$ ). (*Post-Computation*) For  $t > +2$ , the early-to-mid layers retain close to 1 accuracy as they retain the immediate context; the accuracy decreases in the middle layers of the model but not very markedly. Only at the subsequent node ( $t > +5$ ) is the decrease more pronounced.

### B Silent Chain-of-Thought

As stated in the main text we analyzed the *Silent CoT* setting, where the model is forced to compute the answer without explicitly stating the child nodes’ truth value. A representative CoT excerpt can be found in Table S.1.

As seen in Figure S.3, we see that the manifold capacity of the child node increases during the parent’s computation even when the truth values of the child nodes are silenced during the CoT.

Taking a step further, we prompted Ministral to completely silence everything within the line of “\*Logic:” structural token (Table S.2), masking the logic expression, e.g. “[05] and [06]”, with “\*\*\*\*\*”, which has an

---

**Silent CoT example response excerpt**

---

```

...
**Node [19]**
* Logic: '[05] and [06]'
* Result: 'True'
**Node [20]**
* Logic: '[07] xor [08]'
* Result: 'True'
...

```

---

Table S.1

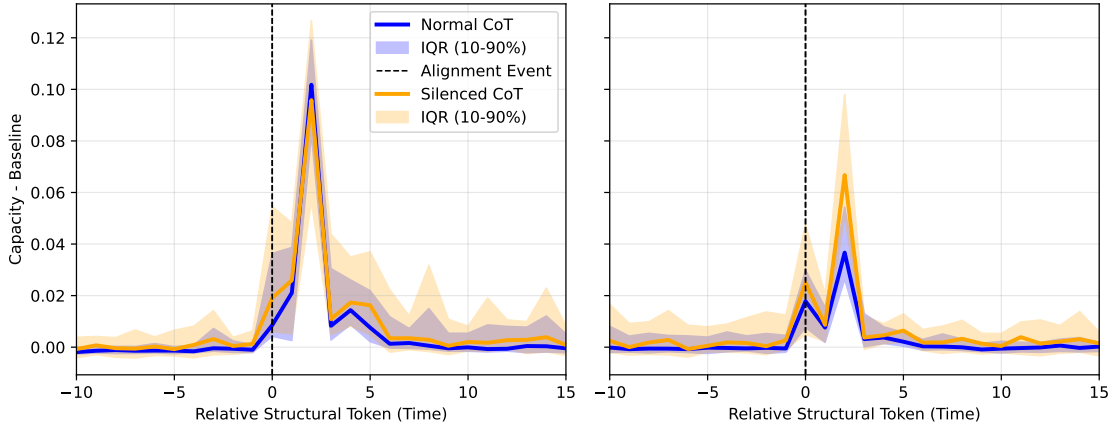


Figure S.3: **Comparison of Capacity dynamics between normal and silenced CoT.** (Left) Data is aligned to the moment a node is computed. There is no statistically significant difference between the two prompts, which is expected as the only difference in the prompts is in the reference to the children. (Right) Data is aligned to the moment a node is recalled by its parent. There is no significant difference between the two prompts, which confirms the linear separability of the children is functionally necessary to compute the parent’s value and does not merely reflect that the children are being recalled.

equal number of tokens. This way, we completely eliminate the possibility of capacity increasing simply due to textual reasons.

---

**Silent CoT example response excerpt**

---

```

...
**Node [19]**
* Logic: '*****'
* Result: 'True'
**Node [20]**
* Logic: '*****'
* Result: 'True'
...

```

---

Table S.2

We find that the capacity of the child node indeed increases during the solve phase of the parent node, despite the absence of any textual output (Figure S.4). We find that the accuracy of the nodes closer to the root node is lower than those closer to the leaf nodes. This naturally leads to lower capacity closer to the root node, a trend clearly visible in Figure S.4, i.e. lower depth (e.g. depth 2) has lower capacity than the higher depth (e.g. depth 5). The positive correlation between the capacity and the accuracies is clearly shown in We find that the capacity of the child node indeed increases during the solve phase of the parent node, despite the absence of any textual output (Figure S.4). We find that the accuracy of the nodes closer to the root node is lower than those closer to the leaf nodes. This naturally

leads to lower capacity closer to the root node, a trend clearly visible in Figure S.4, i.e. lower depth (e.g. depth 2) has lower capacity than the higher depth (e.g. depth 5). The positive correlation between the capacity and the accuracies is clearly shown in Figure S.5. Finally, we also find that the attention map for this case (Figure S.6) is qualitatively the same as the regular prompt case shown in the main text.

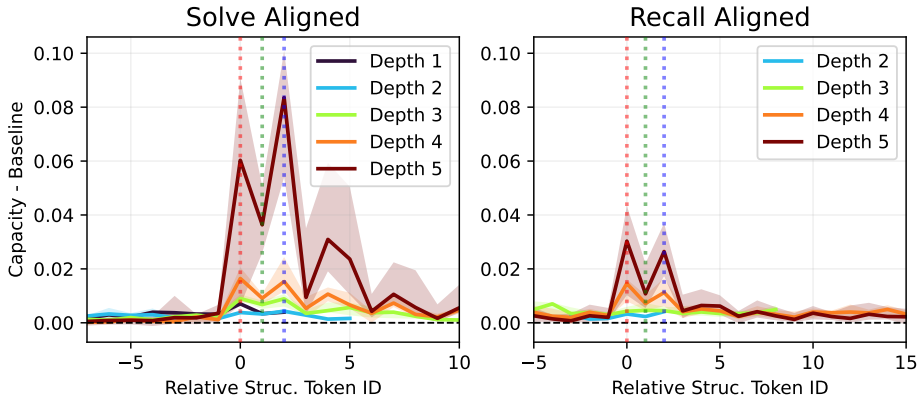


Figure S.4: The masked logic case. Capacity values for each node grouped by the logic tree depth. Left: the node capacity traces aligned at the solve phases of the corresponding nodes. Right: the node capacity traces aligned at the recall phases of the parent nodes (the main focus of this figure).

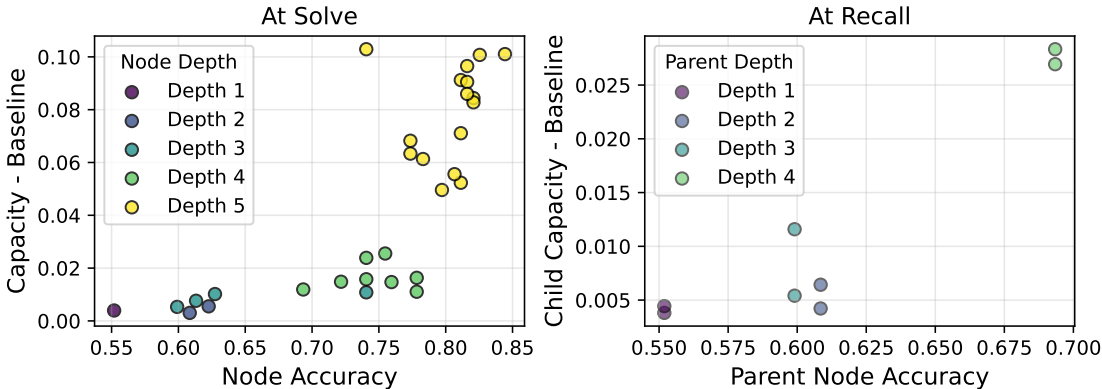


Figure S.5: The masked logic case. Left: node capacity at its solve phase vs. corresponding node accuracy. Right: child node capacity at its recall phase vs. its parent node accuracy.

### C Hyperplane Direction Analysis

We computed the max-margin hyperplanes at each token of interest based on each node’s ground truth labels, and analyzed some pairwise cosine similarities. First, we check if, for all nodes, the manifolds separate along the same direction when they are being solved. It turns out that at the “\*Logic:” token of the solve phase, only the leaf nodes have highly conserved directions, but for the rest, the directions are mostly orthogonal Figure S.7-**top-left**. This reveals that, when a node is being actively solved, each node takes a new orthogonal direction. However, at the “\*Result:” token, all nodes point toward the same direction, presumably the direction that encodes True or False Figure S.7-**bottom-left**.

We also check if the recall direction is conserved across nodes Figure S.7-**middle-and-right**. As noted in the main text, we see that the recall directions are highly conserved across all left child nodes and also for all right child nodes Figure S.7-**right**. Regardless of where in the tree the LM is solving, it treats the left and right child nodes of the node that is being solved equally. This indicates that the LM applies the same local rule to compute all subproblems. These two directions (one for the left child and another for the right child) are slightly anti-correlated.

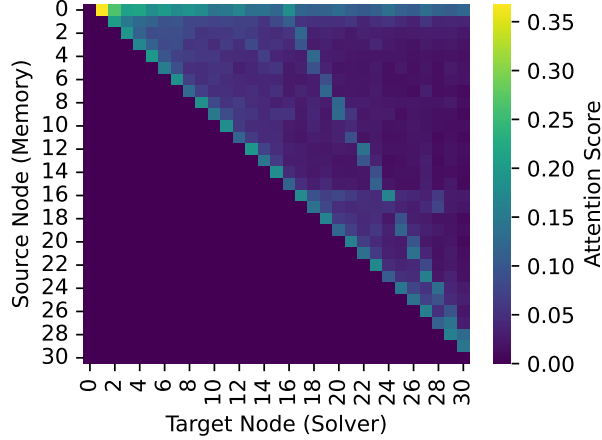


Figure S.6: Attention score heatmap between graph nodes for the masked logic case. The x-axis represents the target node currently being solved; the y-axis represents the source nodes in the context. The diagonal structure reflects the model attending to recent context, while off-diagonal points represent the retrieval of specific dependencies.

Finally, we see if, for a given node, the directions when it is solved and being recalled are conserved. It turns out that the solving and recalling directions are mostly orthogonal Figure S.8.

### D Quantification of Attention Scores

To investigate whether the model retrieves information from previous reasoning steps, we analyze the attention patterns during the “Solve” phase of each parent node. We define the attention score  $A_{T \rightarrow S}$  from a target node  $T$  (the parent) to a source node  $S$  (the child) as follows.

Let  $\mathbf{M}^{(l)} \in \mathbb{R}^{H \times N \times N}$  be the multi-head attention matrix at layer  $l$ , where  $H$  is the number of heads and  $N$  is the sequence length. We identify the set of token indices corresponding to the source node’s solution phase,  $\mathcal{I}_S = \{t \mid \text{token}_t \in \text{Result String of } S\}$ , and the set of token indices corresponding to the target node’s computation phase,  $\mathcal{I}_T = \{t \mid \text{token}_t \in \text{Logic String of } T\}$ .

We compute the maximum attention score across all heads and all token pairs within the defined windows:

$$A_{T \rightarrow S} = \max_{l \in L_{\text{ROI}}} \left[ \max_{h \in \{1 \dots H\}} \left( \max_{i \in \mathcal{I}_T, j \in \mathcal{I}_S} \mathbf{M}_{h,i,j}^{(l)} \right) \right] \tag{1}$$

where  $L_{\text{ROI}}$  represents the layers of interest (e.g., Layer 20). The maximum aggregation is chosen over the mean to detect sparse retrieval mechanisms, as information transfer in transformers is often performed by specialized induction heads rather than distributed uniformly across all heads.

For the correlation analysis shown in Figure 6b, we align this attention score  $A_{T \rightarrow S}$  with the manifold capacity of the source node  $S$ ,  $\alpha^{(S)}$ , measured using the embeddings at the last token of the target phase  $\mathcal{I}_T$ . This allows us to directly compare the strength of retrieval with the resulting linear separability of the retrieved concept.

### E Additional Capacity and Probe Traces

Please see Figures S.9 and S.10.

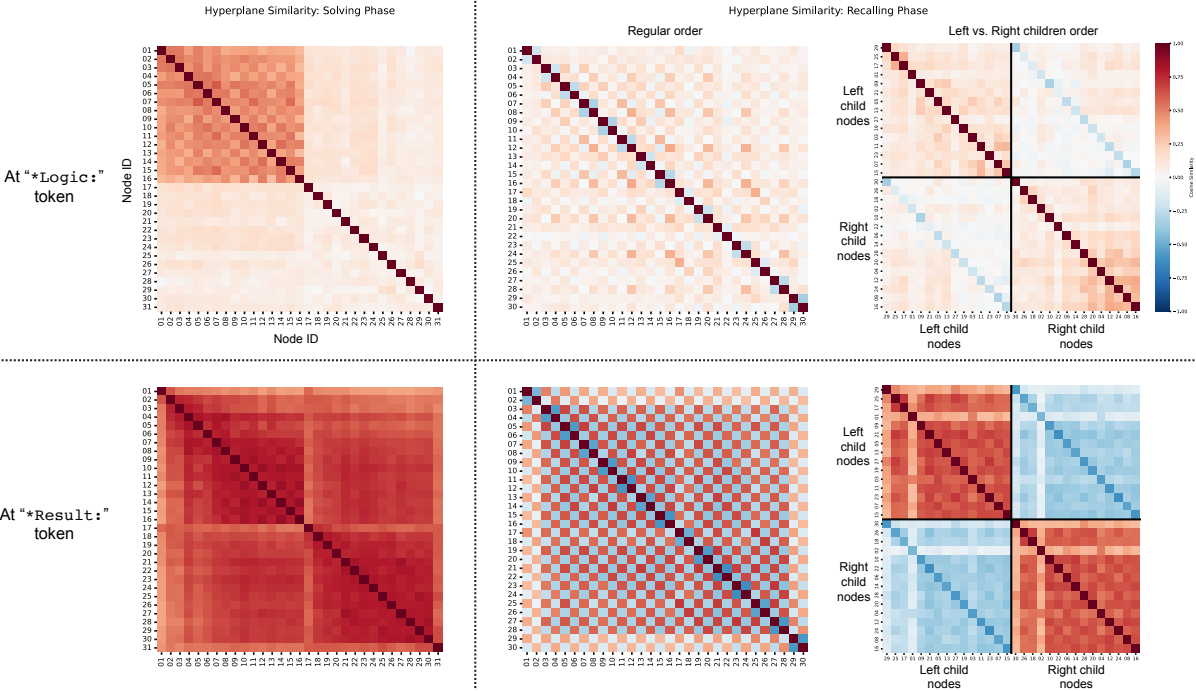


Figure S.7: **Cosine Similarity of Hyperplane Directions between Nodes when They are Solved or Recalled.** Cosine similarity between the max-margin hyperplanes computed for nodes' ground truth answers at the "\*Logic:" tokens (for the **top** row; "\*Result:" tokens for the **bottom** row) in its solve phase (for the **left** column; recalling phase for the **middle** column). For the recall phase similarity, we also show the same plot but with the left and right child nodes grouped, revealing the block structure (the **right** column).

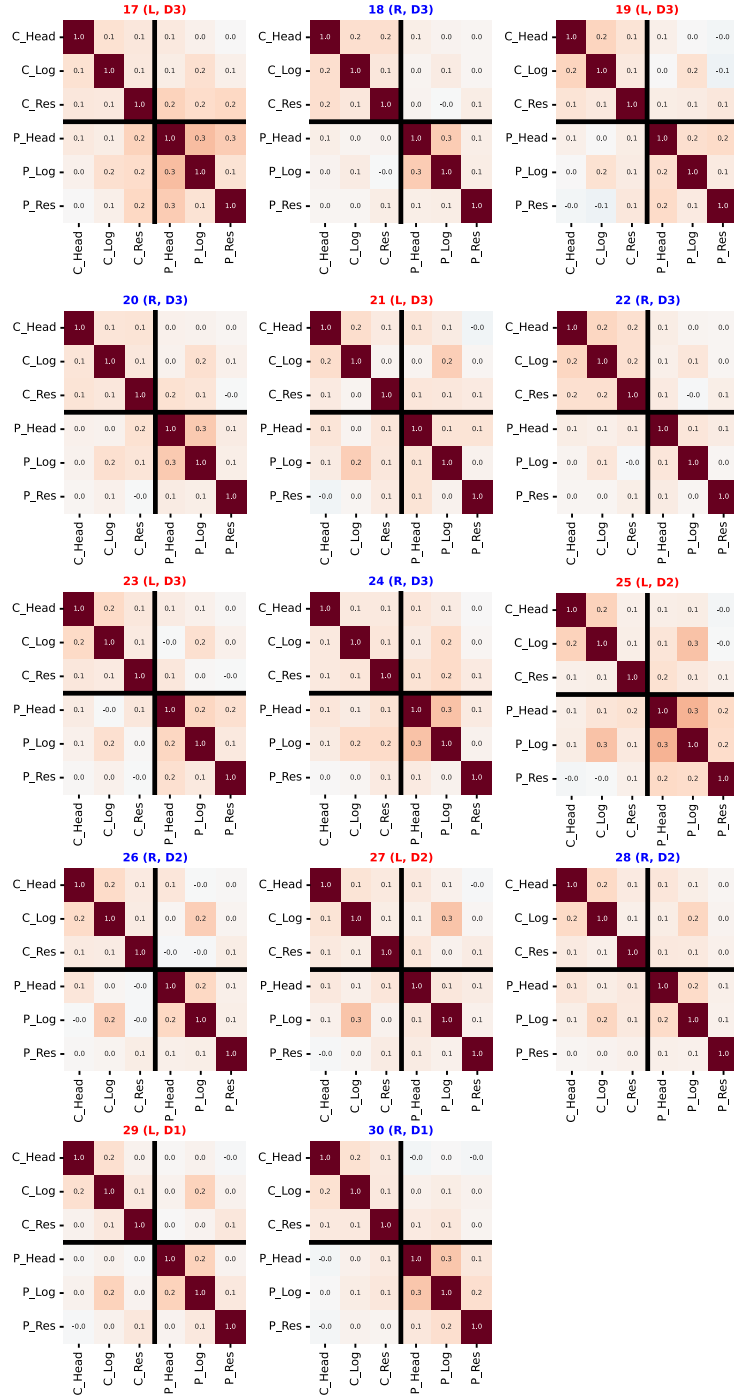


Figure S.8: **Cosine Similarity of Each Node when It is Solved and Recalled.** Cosine similarity between the max-margin hyperplanes computed for a single node's ground truth answer when it is being solved (three structural tokens) and recalled (another three structural tokens).

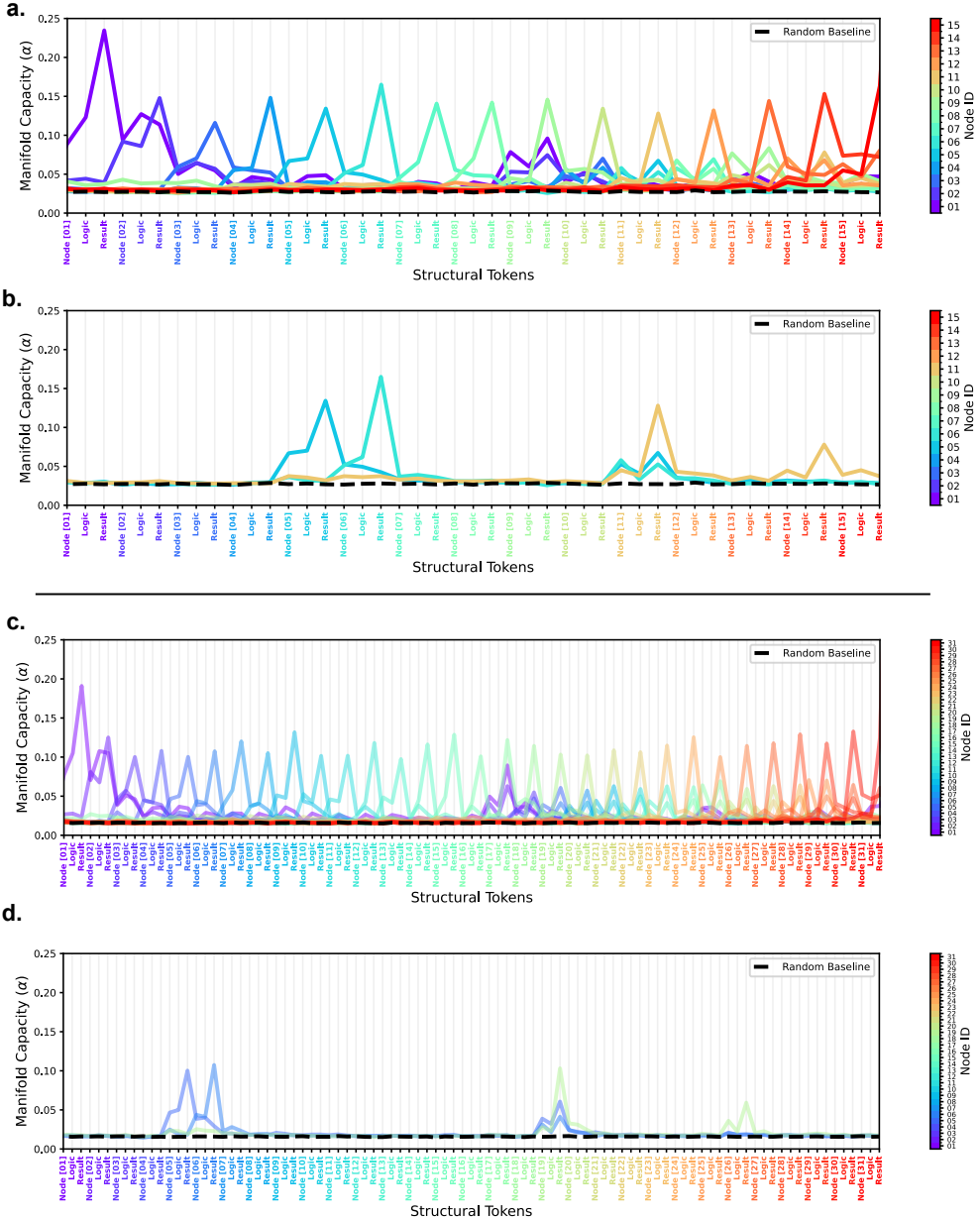


Figure S.9: **Dynamic Modulation of Manifold Geometry during CoT.** **a.** Manifold capacity ( $\alpha$ ) tracked across the Chain-of-Thought sequence (layer 20, tree height  $h = 4$ ). Lines are colored by node ID. Capacity for a specific node peaks sharply at two distinct moments: first when the node is intrinsically computed, and second when it is processed by its parent. **b.** Detailed analysis of Node 11 (yellow) and its children, Node 5 (blue) and Node 6 (turquoise). High capacity peaks correspond to linearly separable manifolds (clear decision boundaries). Notably, representations become entangled (low capacity) in the interim periods between the initial solution (solve) and the subsequent retrieval (recall). **c.d.** *Idem* for a tree of height  $h = 5$

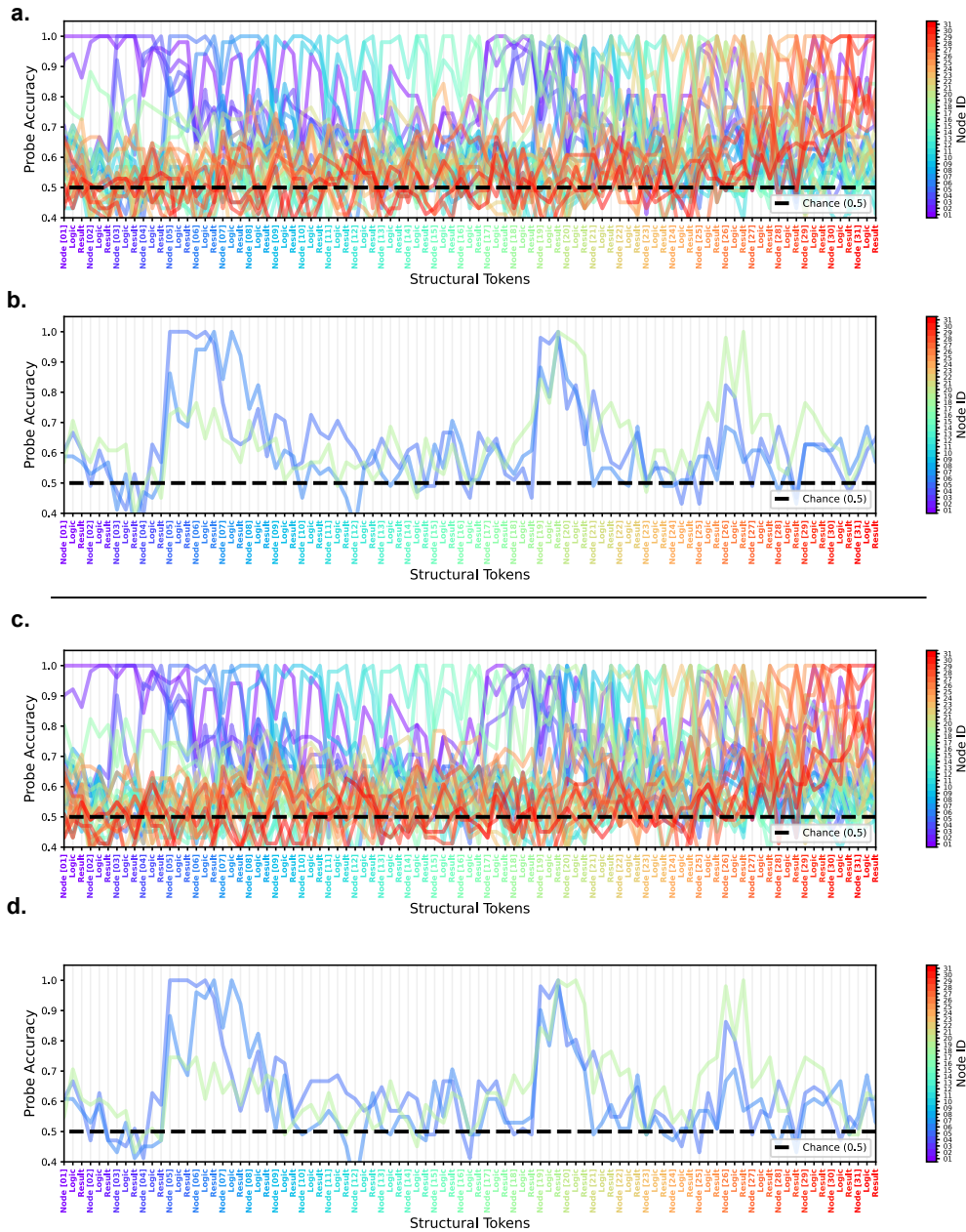


Figure S.10: **Evolution of Linear Probe Test Accuracy during CoT.** **a.** Logistic Probe Test Accuracy across the Chain-of-Thought sequence (layer 20, tree height  $h = 5$ ). Lines are colored by node ID. **b.** Detailed analysis of Node 11 (yellow) and its children, Node 5 (blue) and Node 6 (turquoise). Accuracy peaks at the time each Node is being solved and when it is being recalled. However, contrary to manifold capacity (see Figure S.9cd) the accuracy plateaus for several nodes. **c.d.** *Idem* for a Hard-Margin SVM Probe Test Accuracy.